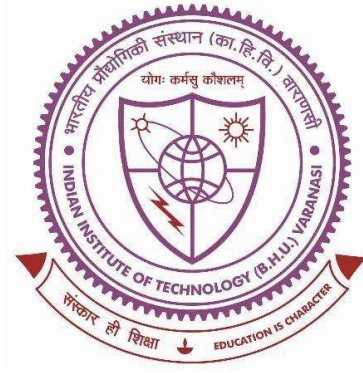


***FRACTURE MECHANICS ANALYSIS OF GIANT
MAGNETOSTRICTIVE MATERIAL IN THE
COUPLED MAGNETO-ELASTIC FIELD***



Thesis submitted in partial fulfilment

for the award of degree

Doctor of Philosophy

by

Praveen Kumar Singh

Department of Mechanical Engineering

Indian Institute of Technology

(Banaras Hindu University)

Varanasi-221005



**INDIAN INSTITUTE OF TECHNOLOGY
(BANARAS HINDU UNIVERSITY),
VARANASI-221005**

CERTIFICATE

This is to certify that the work contained in the thesis titled "*Fracture Mechanics Analysis of Giant Magnetostrictive Material in the Coupled Magneto-Elastic Field*" by "*PRAVEEN KUMAR SINGH*" has been carried out under my/our supervision and that this work has not been submitted elsewhere for a degree. It is further certified that the student has fulfilled all the requirements of Comprehensive Examination, Candidacy and SOTA for the award of Ph.D. Degree.

Co-Supervisor

Dr. Chandana Rath

School of Material Science & Tech.
Indian Institute of Technology (BHU),
Varanasi-221005, India

Associate Professor/सह-आचार्य
School of Materials Sc. & Tech./पदार्थ विज्ञान एवं प्रौद्योगिकी स्कूल
Indian Institute of Technology/भारतीय प्रौद्योगिकी संस्थान
(Banaras Hindu University)/(का.हि.वि.वि.), वाराणसी

Supervisor

Prof. S. K. Panda

Department of Mechanical Engineering
Indian Institute of Technology (BHU),
Varanasi-221005, India

Dr. S. K. Panda
प्राध्यापक/Professor
यांत्रिक अभियंत्रिकी विभाग/Deptt. of Mechanical Engg.
भारतीय प्रौद्योगिकी संस्थान/Indian Institute of Technology
(का० हि० वि०/B. H. U.)
वाराणसी-221005/Varanasi-221005



INDIAN INSTITUTE OF TECHNOLOGY
(BANARAS HINDU UNIVERSITY),
VARANASI-221005

DECLARATION BY THE CANDIDATE

I "**Praveen Kumar Singh**", certify that the work embodied in this thesis is my own bona fide work and carried out by me under the supervision of "**Prof. S. K. Panda**" from " **July 2015** to **DECEMBER 2022**", at the "**DEPARTMENT OF MECHANICAL ENGINEERING**", Indian Institute of Technology (BHU), Varanasi. The matter embodied in this thesis has not been submitted for the award of any other degree/diploma.

I declare that I have faithfully acknowledged and given credits to the research workers wherever their works have been cited in my work in this thesis. I further declare that I have not willfully copied any other's work, paragraphs, text, data, results, etc., reported in journals, books, magazines, reports dissertations, theses, etc., or available at websites and have not included them in this thesis and have not cited as my own work.

Date: 08-02-2023

Place: Varanasi

Praveen

Praveen Kumar Singh

CERTIFICATE FROM THE SUPERVISOR

This is to certify that the above statement made by the candidate is correct to the best of my knowledge.

Chandana Rath

Co-Supervisor

Dr. Chandana Rath

School of Material Science & Tech.
Indian Institute of Technology (BHU)
Indian Institute of Technology (Banaras Hindu University) (का.हि.वि.वि.), वाराणसी

S. K. Panda

Supervisor

Prof. S. K. Panda

Department of Mechanical Engineering
Indian Institute of Technology (BHU)
Varanasi

Santosh Kumar

Prof. Santosh Kumar

Head of Department

Department of Mechanical Engineering,
Indian Institute of Technology (BHU), Varanasi

यांत्रिक अभियान्त्रिकी विभाग/Deptt. of Mechanical Engg.

भारतीय प्रौद्योगिकी संस्थान/Indian Institute of Technology

(का०हि०वि०/B.H.U.)

वाराणसी-221005/Varanasi-221005



INDIAN INSTITUTE OF TECHNOLOGY
(BANARAS HINDU UNIVERSITY),
VARANASI-221005

COPYRIGHT TRANSFER CERTIFICATE

Title of the Thesis: *Fracture Mechanics Analysis of Giant Magnetostrictive Material in The Coupled Magneto-Elastic Field*

Name of the Student: PRAVEEN KUMAR SINGH

Copyright Transfer

The undersigned hereby assigns to the Indian Institute of Technology (Banaras Hindu University) Varanasi all rights under copyright that may exist in and for the above thesis submitted for the award of the "**DOCTOR OF PHILOSOPHY**".

Date: 08-02-2023

Place: Varanasi

Praveen
(PRAVEEN KUMAR SINGH)

Note: However, the author may reproduce or authorize others to reproduce material extracted verbatim from the thesis or derivative of the thesis for author's personal use provided that the source and the Institute's copyright notice are indicated.

Abstract

Giant magnetostrictive materials (GMM) exhibit nonlinear magneto-thermo-elastic coupling phenomena and possess such distinctive properties as high saturation magnetostriction, variable elastic modulus, high curie temperature and faster response to operational factors, thereby finding potential applications in sensing and actuation field. Taylor series expansion of Gibbs free energy density function for elastic deformation, the physics of demagnetization and the Weiss molecular field coupled with the thermodynamic relations have been used to develop a generalized nonlinear hysteretic thermo-magneto-elastic vector model with potential application for the development of sensors and actuators. The nonlinear elastic strains in the magnetostrictive material are induced due to the magnetic domain rotation caused by tensile and compressive stresses in giant magnetostrictive materials. A vector function of the hyperbolic tangent is defined to take into account this nonlinear characteristic validating the elastic stress field boundary condition. The vector generalized Jiles-Atherton hysteresis model with modified Langevin equation is employed to incorporate the pinning of magnetic domain walls in the mathematical model. Thus, derived macroscopic model is put to the test for 1D, 2D and 3D nonlinear magnetostriction, magnetization and elastic constitutive relation with Terfenol-D (giant magnetostrictive materials) as a potential candid material. Finite element analyses for rods and films have been conducted using the general $\mathbf{H}(\mathbf{B})$ relation coded in the C programming language. Employing the calibrated physical and experimental parameter, the confidence of the model is checked with existing analytical and experimental models. The magnetization and magnetostriction hysteresis responses have been evaluated considering the variation of a broad range of the prestress (up to 110 MPa), temperature (0 °C to 80 °C) and applied magnetic field (0 A/m to 193.2 kA/m).

The numerical simulation of this fully coupled phenomenological model demonstrates good agreement with the experimental data. The theoretical modelling error obtained from averaging the normalized root mean square error for each experimental data set is found to be maximum of 2.8 % and hence vindicates the efficacy of the present model.

Then, the proposed the generalized nonlinear hysteretic thermo-magneto-elastic constitutive model is used to derive a universal path independent integral that represents the energy release rate or flux during crack extension in a homogeneous and isotropic material for mode I fracture problem. This version of integral includes the effect of elastic strain, thermal strain, body forces and magnetic strain. Particularly focus is made on magneto-thermo-elastic strains. Some physics-based experiments for magnetization and magnetostriction hysteresis loops and mechanical compression tests under the applied magnetic field are conducted for Terfenol-D based specimens. A finite element study is performed using the proposed constitutive model and consequently, numerical results are compared with experiments to optimize the material parameters. The single edge notch bend (SENB) specimen is subjected to three-point flexure testing in the absence and presence of an external magnetic field in accordance with ASTM E399. The digital image correlation technique is used to capture the load line and crack opening displacement variation peak fracture load data. Two parameter Weibull statistical theory of strength has been utilised to forecast the mean peak fracture load. The Weibull modulus and goodness of fit are assessed using linear regression analysis (LIN2), biased and unbiased maximum likelihood estimation (MLE2-B & MLE2-U) approach. A finite element model based on optimized nonlinear constitutive relations is built concerning to magnetization and stress dependent elasticity problem of Terfenol-D fracture. Critical strain energy release rate J_{Ic} was calculated using the mean peak fracture load in both absence and presence of the external magnetic field. The influence of bi-nonlinear modularity and applied external

magnetic field on the fracture behaviour of the Terfenol-D SENB specimen were compared with the unimodular experimental results and substantial difference was reported. The stipulation and importance of considering the bi-nonlinear critical strain energy release rate J_{Ic} in the context of a coupled magneto-elastic field was discussed in detail.

Finally, a combined numerical and experimental study has been conducted to understand the influence of magnetic fields on the cyclic fatigue behavior of Terfenol-D. A three-point flexure fatigue experimental scheme is employed to evaluate the propagation of crack growth with the number of cycles in Terfenol-D SENB specimen with the absence and presence of an external magnetic field as per ASTM standards (i.e., E399 and E 647). A finite element simulation procedure is used to determine the updated Paris law constants from the correlation of the crack growth rate with the values of ΔJ for a particular set of load ratio, magnetic field, and cyclic frequency. The experimentally and numerically evaluated fatigue failure data with the number of cycles spent were then compared to determine the validation and relevance of evaluated Paris law constants.

This Page is Intentionally Left Blank

Acknowledgements

Let me begin by expressing my gratitude to God, the almighty, for propelling me into this degree of intellectual study. Following this, I feel a sense of pride and pleasure at having the opportunity to express my gratitude to those who have contributed so much to this research project. It is my great honour to remember the few individuals whose enormous grit and determination made this possible and to express my gratitude for everything they have done to make this dream a reality.

First and foremost, I express my sincere thanks and gratitude beyond words to my esteemed supervisors, Prof. S. K. Panda and Dr. Chandana Rath for their consistent help, encouragement, and valuable discussions during the entire period of my research work. It would not have been possible to complete the thesis without his utmost involvement and invaluable efforts. They motivated me to pursue the research problem and the need for persistent effort to accomplish the goal. I am truly indebted to him.

Besides my supervisor, I would like to thank my RPEC members, Dr. M. R. Majhi of Ceramic engineering and Dr. D. Khan of Department of Mechanical Engineering for their insightful comments and encouragement. I sincerely thank Prof. Santosh Kumar, Head of the Department of Mechanical Engineering and all the former heads for providing all the research facilities to successfully accomplish my research in the department. I have deep sense of gratitude to all the faculty members especially, Prof. V. P. Singh, Prof. Rajesh Kumar, Prof. Sandeep Kumar, Prof. R. K. Gautam, Prof. A. P. Harsha and Dr. Amit Tyagi of the Department of Mechanical Engineering, IIT (BHU), Varanasi for their cooperation and inspiration.

I wish to acknowledge my sincere gratefulness to Prof. Santosh Kumar, Head, Department of Mechanical Engineering, Indian Institute of Technology (BHU), Varanasi, the former heads Prof. A. P. Harsha, Prof. A. K. Jha, Prof. A. K. Agrawal for their kind gesture and extending all sorts of facilities in the Department to pursue this kind of research work. I am also thankful to Convener DPGC, Dr A. Sarkar and all respected DPGC members for their kind support.

I am very obliged to my seniors Dr Awani Bhushan and Dr Sanjeev Kumar Singh for engaging me in fruitful discussions on my research work and encouraging me throughout the work. Special thanks to my colleagues at Strength of Material laboratory Mr. Ashish Singh Pareta, Mr. Anupam Tiwari, Mr. Saurabh Chauhan, Mr. Ravindra Soni and Mr. Shashi Ranjan. I am also thankful to all my friends: Himanshu Tiwari, Dr Ankitendran Mishra, Dr Nitesh Gupta, Satish Upadhyay, Dr Varun Sonker and Dr Dhiraj Kumar for their constant encouragement and for being with me in my moments of happiness and troubles at IIT (BHU), Varanasi.

I would like to express my deepest gratitude to my parents Mrs. Manju Singh and Mr. Raj Kumar Singh for their unconditional support and encouragement to pursue my interest. I would also like to thank my wife Mrs. Anukriti Singh, brother Mr. Saurabh Kumar Singh and family members Mr. S. K. Singh, Mrs. Deepika Singh, Mrs. Aayushi Singh, Mr. Rakshit for their consistent support and encouragement throughout this journey.

Last but not the least, I wish to thank my friends and the persons whose names have not been mentioned on this piece of paper for extending their cooperation directly or indirectly.

Praveen Kumar Singh

Contents

<i>Abstract</i>	<i>i</i>
<i>Acknowledgements</i>	<i>v</i>
<i>Contents</i>	<i>vii</i>
<i>List of Figures</i>	<i>xiii</i>
<i>List of Tables</i>	<i>xxiii</i>
<i>Nomenclature</i>	<i>xxv</i>
<i>Preface</i>	<i>xxix</i>
Chapter 1. Introduction	1
1.1. Overview and motivation.....	1
1.1.1. Giant magnetostrictive materials (GMM).....	5
1.1.2. Fracture and Fatigue failure of giant magnetostrictive materials	9
1.1.3. Constitutive modelling.....	13
1.2. Research objectives.....	17
1.3. Scope of research	19
1.4. Dissertation outline	21
Chapter 2. Theoretical Background	25
2.1. Magnetism.....	25
2.1.1. Magnetic Field	26
2.1.2. Magnetic moment and Magnetization	26
2.1.3. Magnetic flux density and hysteresis loops	27
2.1.4. Exchange and Magnetic energy	30

2.1.5.	Demagnetization energy	31
2.1.6.	Magnetization processes	31
2.1.7.	Magnetic anisotropy	33
2.1.8.	Magnetostriction.....	34
2.1.9.	Maxwell equations	37
2.1.10.	Magnetic scalar and vector potentials	38
2.1.11.	Boundary conditions	40
2.2.	Nonlinear elasticity.....	43
2.2.1.	Stress-strain relations	44
2.2.2.	Equilibrium equation.....	45
2.3.	Magneto-elastic failure	46
2.3.1.	Fracture.....	47
2.3.2.	Fatigue.....	50
2.4.	Weibull strength theory	53
Chapter 3. A Novel Magneto-Thermoelastic Constitutive Model.....		55
3.1.	Introduction	55
3.2.	Coupled Nonlinear Hysteretic Constitutive Relationship	56
3.2.1.	Mathematical framework	57
3.3.	Qualitative Discussion.....	63
3.3.1.	On tensors S_{ijkl} and m_{ijkl}	63
3.3.2.	On $\lambda_{0ij}(\sigma_{mn})$ and $f_k^{-1}(M)$	64
3.4.	Simplified Hysteretic Constitutive Model.....	66
3.4.1.	2-D model for magnetostrictive thin films and plates.....	72
3.4.1.1.	For magnetic field parallel to film/plate	73

3.4.1.2.	For magnetic field perpendicular to film/plate.....	74
3.4.1.3.	For magnetic field parallel to film (Along the x -direction).....	75
3.4.1.4.	For magnetic field perpendicular to film (Along the z -direction).....	76
3.4.2.	1-D model for magnetostrictive rods.....	76
3.4.3.	Solution Algorithm.....	77
3.5.	Simulation Physics.....	79
3.5.1.	Model Definition.....	80
3.5.1.1.	For actuators based on rods.....	81
3.5.1.2.	For actuators based on films.....	81
3.6.	Verification With Experiments And Discussions.....	82
3.6.1.	Case Study 1: For magnetostrictive rods.....	84
3.6.2.	Case Study 2: For magnetostrictive thin films.....	99
3.7.	Summary.....	110
<i>Chapter 4. Three-Dimensional Path Independent Integral for Coupled Magneto-Thermo-Elastic Fracture Domain.....</i>		<i>113</i>
4.1.	Introduction.....	113
4.2.	Formulation of the path independent 3D J-Integral.....	114
4.2.1.	Coupled Magneto-Thermo-Elastic field contribution in J-integral.....	117
4.3.	Summary.....	122
<i>Chapter 5. Numerical and experimental analysis for calibration of the magneto-elastic material parameters.....</i>		<i>123</i>
5.1.	Introduction.....	123
5.2.	Experimental characterization.....	124

5.2.1.	Hysteretic magnetic response characterization set up	124
5.2.2.	Magneto-elastic compression test	126
5.3.	Numerical Analysis	128
5.3.1.	Solution method in COMSOL.....	131
5.3.2.	Numerical model for magneto-elastic response of material.....	132
5.4.	Results and Discussions.....	133
5.4.1.	Comparison between hysteretic magnetic response experiments and simulation.....	134
5.4.2.	Comparison between compression experiment and simulation	136
5.5.	Summary.....	138
<i>Chapter 6. An experimental and numerical study for Mode I fracture parameter characterization of a cracked giant magnetostrictive material</i>		<i>139</i>
6.1.	Introduction	139
6.2.	Fracture toughness experiment.....	141
6.3.	Experimental evaluation of strain energy release rate J_{Ic}	144
6.3.1.	For unimodular material	144
6.3.2.	For variable modulus material.....	146
6.4.	Numerical model for Terfenol-D SENB specimen	147
6.4.1.	Finite element computation procedure for J-integral	151
6.5.	Results and discussions	154
6.5.1.	Weibull statistical theory in the estimation of peak fracture load.....	157
6.5.2.	Experimental results for J_{Ic}	164
6.5.3.	Numerical results for J_{Ic}	165

6.6. Summary	180
Chapter 7. An experimental and numerical analysis for fatigue strength characterization and life prediction of giant magnetostrictive material.....	183
7.1. Introduction	183
7.2. Fatigue experiment.....	185
7.3. Numerical model.....	190
7.3.1. Computation of J -Integral.....	193
7.4. Results and discussions	195
7.4.1. Experimental results for crack growth.....	195
7.4.2. Numerical determination of updated Paris law constants.....	196
7.4.3. Numerical fatigue life prediction and experimental validation	203
7.5. Summary	209
Chapter 8. Conclusions and Future scope.....	211
8.1. General conclusions	211
8.2. Future scopes.....	217
References	219
Appendix A.....	230
List of Publications	233

This Page is Intentionally Left Blank

List of Figures

Figure 1.1 Terfenol-D based Transducer. Reprinted with kind permission from [3].	2
Figure 1.2 Magnetostrictive vibration energy harvester for power generating floor systems [6] © [2015] IEEE.	2
Figure 1.3 Three magnetostrictive actuators were attached to the strut of helicopter externally by means of a collar for active vibration suppression. Reprinted from Journal of Sound and Vibration, 205(1), T. J. Sutton, S. J. Elliott and M. J. Brennan, Active isolation of multiple structural waves on a helicopter gearbox support strut, 81-101, copyright (1997), with permission from Elsevier [7].	3
Figure 1.4 Active control of Gearbox vibration with two pairs of magnetostrictive actuators supporting the bearing [8].	4
Figure 1.5 Magnetization curves of Terfenol-D at different temperature levels. Reprinted from [13] [Clark AE, Teter JP, McMasters OD. Magnetostriction “jumps” in twinned Tb _{0.3} Dy _{0.7} Fe _{1.9} . J Appl Phys 1988;63:3910–2], with the permission of AIP Publishing.	6
Figure 1.6 Magnetostriction curves of Terfenol-D at different temperature levels. Reprinted from [13] [Clark AE, Teter JP, McMasters OD. Magnetostriction “jumps” in twinned Tb _{0.3} Dy _{0.7} Fe _{1.9} . J Appl Phys 1988;63:3910–2], with the permission of AIP Publishing.	7
Figure 1.7 Strain vs stress loop for DC applied field levels H (0–193.2 kA/m at 16.1 kA/m steps). Reprinted with kind permission from [17].	7
Figure 1.8 Young’s Modulus for DC applied field levels H (0–193.4 kA/m at 16.1 kA/m steps) Reprinted with kind permission from [17].	8
Figure 1.9 Stress-strain curve for Terfenol-D rod when magnetization $M = 0$. Where, $\lambda_0\sigma$ is Stress Dependent Nonlinear Strain caused by the Magnetic Domain Rotation and λ_s is Saturated Magnetostriction	11

Figure 2.1 Typical experimental $B-H$ loop of a ferromagnetic material	28
Figure 2.2 A typical $M-H$ curve of a ferromagnetic material.....	29
Figure 2.3 Schematic diagram showing the magnetostriction in: (a) the ordered but misaligned demagnetized ferromagnetic regime; and (b) the ordered and aligned ferromagnetic regime, magnetized to saturation.	35
Figure 2.4 Interface between two medium.....	41
Figure 2.5 The magnetic insulation boundary condition.....	42
Figure 2.6 The perfect magnetic conductor boundary condition	42
Figure 2.7 Elastic stress-strain curve for (a) linear material (b) bi-linear material and (c) nonlinear material.....	44
Figure 2.8 Fracture mode (I) Opening mode (II) Sliding mode (III) Tearing mode	48
Figure 2.9 Counter-clockwise contour for 2D J-integral	49
Figure 2.10: Cyclic loading	50
Figure 2.11 Stages of fatigue crack growth.....	52
Figure 3.1 A schematic diagram of the nonlinear part of elastic strain (λ_0) vs. the stress (σ) curve for a giant magnetostrictive material.	64
Figure 3.2 A solution algorithm for the generalized coupled nonlinear hysteretic constitutive model for major hysteresis loops.....	78
Figure 3.3: 2D axisymmetric geometry of actuator based on Terfenol-D rod with (a) mapped meshing of the actuator and (b) magnetic flux density distribution along the longitudinal direction of Terfenol-D rod in COMSOL Multiphysics	81
Figure 3.4: 3-D geometry of actuator based on Terfenol-D film with (a) meshing of the actuator and (b) magnetic flux density norm distribution in COMSOL Multiphysics	82
Figure 3.5: Comparison of compressive strain vs compressive stress curves predicted by the proposed constitutive model and Jin et al. model[54] with Kellogg et al. experimental results[17] ($H=193.2$ kA/m) at room temperature.....	85

Figure 3.6: Comparison of the Magnetostriction hysteresis curves predicted by the proposed constitutive model under different pre-stresses with Moffett’s experimental results[14] at room temperature.	86
Figure 3.7: Comparison of the Magnetostriction hysteresis curves predicted by the proposed constitutive model without considering the Weiss field parameter under different pre-stresses with Moffett et al. experimental results[14] at room temperature.	87
Figure 3.8 (a) Piezomagnetic coefficient vs magnetic field under various prestress (Scatters: Moffett et al. experimental results [14] ; solid lines: theoretical predictions) (b) Piezomagnetic coefficient vs compressive stress under different magnetic field levels.	88
Figure 3.9: Magnetization and Magnetostriction hysteresis curves predicted by the proposed constitutive model under different pre-stresses at room temperature up to saturation (a) magnetization vs. applied magnetic field (b) magnetostriction vs applied field	90
Figure 3.10: Comparison of the Magnetization and Magnetostriction hysteresis curves predicted by the proposed constitutive model under various ambient temperatures with Clark et al. experimental results[13] at 13.3 MPa compressive pre-stress. (Dashed lines: experimental curves; solid lines: theoretical predictions).....	91
Figure 3.11: Comparison of compressive strain vs compressive stress curves predicted by the proposed constitutive model with Kellogg et al. experimental results[17] at room temperature (Dashed lines: experimental curves; solid lines: theoretical predictions)	93
Figure 3.12: Comparison of Young’s modulus vs compressive stress curves predicted by the proposed constitutive model with Kellogg et al. experimental results[17] under different magnetic fields levels at room temperature. (Scatters: experimental curves; solid lines: theoretical predictions)	94

Figure 3.13: Predicted Young’s modulus vs magnetic field curves under various compressive stresses at room temperature	95
Figure 3.14: Predicted Young’s modulus vs magnetic field curves under different temperatures at $\sigma = -28$ MPa.....	96
Figure 3.15: Predicted symmetric hysteresis inner loops for Magnetization vs Magnetic Field curves at $\sigma = -28$ MPa and room temperature a) inner hysteresis loops b) Zoomed view of the earmarked loop.....	97
Figure 3.16: Comparison of predicted magnetization vs. internal magnetic field hysteresis curves by the proposed constitutive model and Jin et al. model [54] with Schatz’s experimental results[16] for a film with in-plane tensile stress subjected to transverse magnetic field.....	100
Figure 3.17: Comparison of predicted magnetization vs. internal magnetic field hysteresis curves with Schatz’s experimental results[16] for a film under (a) tensile stress and (b) compressive stress at room temperature	101
Figure 3.18: Comparison of predicted magnetostriction parallel to film plane vs. applied magnetic field hysteresis curves with Schatz’s experimental results[16] for a film at room temperature.	103
Figure 3.19: Predicted magnetization vs. internal magnetic field hysteresis curves at different in-plane stress levels, when subjected to in-plane applied field.....	104
Figure 3.20: Predicted magnetization vs. internal magnetic field (hysteresis curves at different in-plane stress levels, when subjected to transverse applied field.....	105
Figure 3.21: Predicted magnetostriction parallel to film plane vs. applied magnetic field hysteresis curves at different in-plane stress levels.....	106
Figure 3.22: Predicted magnetization vs. internal magnetic field hysteresis curves at different temperatures (Solid lines: for in-plane applied field; Dashed lines: for transverse applied field)	107

Figure 3.23: Predicted magnetostriction parallel to film plane vs applied magnetic field hysteresis curves at different temperatures	107
Figure 3.24: Effect of demagnetization factor on (a) magnetization vs. internal magnetic field hysteresis curves with Schatz’s experimental results [16] (b) magnetostrictive strain vs. applied magnetic field curves for a film with in-plane tensile stress subjected to transverse magnetic field at room temperature.	108
Figure 4.1 Configuration of three-dimensional crack front in solid; A2: fracture process region	115
Figure 4.2 Arbitrary integration contour perpendicular to crack front at O, in the plane $X_3 = 0$	115
Figure 4.3 Stress-strain curves predicted by the constitutive model at different magnetic field levels when $N_{xx} = 0.096$	117
Figure 5.1 (a) Experimental arrangement for magnetization and magnetostriction test (b) Terfenol-D sample with pickup coils and Hall probe in a zoomed-in perspective (c) Terfenol-D sample with strain gauge and Hall probe in a zoomed-in perspective	125
Figure 5.2: (a) Coupled field compression test setup (b) Zoomed view of Hall probe and solenoid (c) Arrangement of Terfenol-D rod specimen inside the solenoid in a zoomed-in perspective.	127
Figure 5.3 A solution algorithm for the coupled nonlinear hysteretic constitutive model for evaluating material’s nonlinear responses	129
Figure 5.4: Schematic diagram of multiphysics calculation module for coupled magneto-elastic response of Terfenol-D.....	131
Figure 5.5: Mapped meshing and magnetic flux density distribution along the longitudinal direction of Terfenol-D rod in the 2D axisymmetric space.....	133
Figure 5.6 Comparison of magnetostriction curves obtained by the present experiment with the Moffett et al.’s [14] experiment at different pre-stress levels.....	133

Figure 5.7 Comparison of the Magnetization and Magnetostriction hysteresis curves predicted by the constitutive model under various pre-stress levels with experimental results at room temperature. (Dashed lines: experimental curves; solid lines: theoretical predictions)	135
Figure 5.8 (a) Comparison of compressive strain vs compressive stress curves predicted by the constitutive model with the experimental results at room temperature (Scatters: experimental curves; solid lines: theoretical predictions) (b) Young's modulus vs compressive stress curves	137
Figure 6.1 Experimental setup for fracture toughness test of single edge notch bend (SENB) specimen in three-point loading under magnetic field	141
Figure 6.2 (a) Specimens geometry (b) Enlarged view of the notch edge as per ASTM standard	142
Figure 6.3 Force vs. crack mouth displacement curve for random Terfenol-D specimen	144
Figure 6.4 Load-displacement curves showing elastic component of absorbed energy U_{el}	146
Figure 6.5 Quarter symmetric FE model for single edge specimen in three-point bending (symmetry regions are shaded in blue colour)	148
Figure 6.6: <i>Interface between two mediums.</i>	148
Figure 6.7: (a) <i>The magnetic insulation boundary condition</i> (b) <i>The perfect magnetic conductor boundary condition</i>	149
Figure 6.8 FE mesh distribution for the quarter symmetric numerical model of the single edge three-point bend specimen under the externally applied magnetic field (a) air domain comprising the specimen (b) quarter symmetric specimen (c) enlarge view of mesh near the crack tip	150
Figure 6.9 Contours for J-integral evaluation	153

Figure 6.10: The probability density function plot with random peak fracture load dataset obtained for the Terfenol-D SENB specimens (a) in absence of magnetic field and (b) in presence of 0.03 T magnetic field using Weibull and Normal distribution.....	159
Figure 6.11: Weibull distribution plot for peak fracture load dataset obtained for the Terfenol-D SENB specimens and the best fit line drawn with LIN2, MLE2-B and MLE2-U estimators (a) in absence of magnetic field (b) in presence of 0.03 T magnetic field.	160
Figure 6.12: Experimental energy release rate J_{Ic} values based on the elastic component of absorbed energy with respect to peak fracture load	164
Figure 6.13: Von-Mises stress (in Pa) distribution in the quarter symmetric Terfenol-D specimen at 0.03T and subjected to mean peak load 46.616N	166
Figure 6.14: Magnetization (in A/m) distribution in the quarter symmetric Terfenol-D specimen at 0.03 T and subjected to mean peak load 46.616 N.	166
Figure 6.15: Comparison of stress (in Pa) component in x-direction distribution at the mid-plane of numerical specimen when subjected to load 46.616N (a) in absence of magnetic field (b) in presence of 0.03 T magnetic field.	167
Figure 6.16: Stress (in Pa) component in x-direction distribution at the mid-plane of numerical specimen (a) in absence of magnetic field and subjected to fracture load 54.134N (b) in presence of 0.03 T magnetic field and subjected to fracture load 46.616N.....	168
Figure 6.17: Variation of $J_{1C} + J_{2C}$ at different cross-sectional planes under (a) $B_0 = 0.03$ T and (b) $B_0 = 0$ T	170
Figure 6.18: Variation of J_{2A} and J_{3A} at different cross-sectional planes under (a) $B_0 = 0.03$ T and (b) $B_0 = 0$ T	171
Figure 6.19: Variation of $J_{1C} + J_{2C} + J_{2A} + J_{3A}$ at different cross-sectional planes under (a) $B_0 = 0.03$ T and (b) $B_0 = 0$ T.....	172

Figure 6.20: Variation of J_{1A} at different cross-sectional planes under (a) $B_0 = 0.03$ T and (b) $B_0 = 0$ T	173
Figure 6.21: Path independence of 3-D J-integral, J_{1n} , at different cross-sectional planes under (a) $B_0 = 0.03$ T and (b) $B_0 = 0$ T	174
Figure 6.22: Distribution of 3-D J-integral, J_{1n} , across the thickness	176
Figure 6.23: 3-D J-integral, J_{1n} , at mid-plane vs load point displacement (Solid lines: 3-D J-integral at mid-plane; Dashed line: 2-D plane strain)	176
Figure 7.1: Experimental setup for fatigue strength characterization of single edge notch bend (SENB) specimen in three-point loading under magnetic field	186
Figure 7.2: Specimens geometry as per ASTM E399-18a standard	187
Figure 7.3: DIC setup	187
Figure 7.4: Cyclic compressive loading	188
Figure 7.5: Mode I fatigue crack in Terfenol-D specimen	189
Figure 7.6: <i>Half symmetric 2-D FE model for single edge specimen in three-point bending</i>	190
Figure 7.7: FE mesh distribution for the half symmetric numerical model of the single edge three-point bend specimen under the externally applied magnetic field (a) air domain comprising the specimen (b) half symmetric numerical specimen (c) enlarge view of mesh near the crack tip	192
Figure 7.8: Direction of constant external magnetic field ($B_0 = 0.03$ T)	193
Figure 7.9 Variation of crack advancement vs number of cycles	196
Figure 7.10: Determination of slope of curve at any random point by secant method	198
Figure 7.11: Numerical scheme for evaluation of ΔJ with the variation in crack growth	199
Figure 7.12: Von mises stress (in Pa) distribution in the half symmetric Terfenol-D specimen at 0.03 T subjected to -40 N	200

Figure 7.13: Magnetization norm (in A/m) distribution in the half symmetric Terfenol-D specimen at 0.03 T subjected to -40 N.....	200
Figure 7.14: Stress (in Pa) component in x-direction distribution in the half symmetric Terfenol-D specimen at 0.03 T subjected to -40 N.....	201
Figure 7.15: Comparison of stress (in Pa) component in x-direction distribution in the numerical specimen when subjected to load -40 N (a) in absence of magnetic field (b) in presence of 0.03 T magnetic field.	201
Figure 7.16: Fatigue crack growth rate as a function of strain energy release rate range ΔJ	202
Figure 7.17: Numerical scheme for evaluation of fracture load data with the number of cycles spent.....	204
Figure 7.18 Maximum load versus number of cycles to failure of Terfenol-D	206

This Page is Intentionally Left Blank

List of Tables

Table 3-1: Normalized root mean square errors (average and maximum errors) obtained with the coupled nonlinear hysteretic model	83
Table 3-2: Optimized model parameters for different experimental data sets	84
Table 3-3: Material Parameters of Terfenol-D amorphous films	100
Table 5-1 Material properties of the Terfenol-D specimens.....	136
Table 6-1 Peak fracture load datasets obtained from (SE) three-point flexure experiments.....	156
Table 6-2: Co-efficient of determination (R^2), Weibull modulus and mean characteristic load parameter with Weibull distribution in different externally applied magnetic field.	163
Table 6-3: Mean experimental critical energy release rate J_{Ic} values	164
Table 6-4: Critical energy release rate J_{Ic} values in 3D and 2D non-linear elastic computation.	177
Table 7-1: Fatigue-fracture load data in presence of the magnetic field 0.03 T.....	207
Table 7-2: Fatigue-fracture load data in presence of the magnetic field 0.03 T.....	208

This Page is Intentionally Left Blank

Nomenclature

Acronyms

GMM	Giant Magnetostrictive Material
SENB	Single Edge Notch Bend
FE	Finite Element
J-A	Jiles-Atherton
LIN2	Linear Regression Analysis (For two parameter Weibull statistical distribution)
MLE2-B	Maximum Likelihood Estimator- Biased (For two parameter Weibull statistical distribution)
MLE2-U	Maximum Likelihood Estimator- Unbiased (For two parameter Weibull statistical distribution)

Greek characters

ν	Poisson's ratio
σ_{ij}	Total Stress Tensor
$\tilde{\sigma}_{ij}$	Effective Stress Tensor
$ \tilde{\sigma} $	Max ($ \tilde{\sigma}_{xx} , \tilde{\sigma}_{yy} , \tilde{\sigma}_{zz} $)
σ_s	Saturation Stress
ε_{ij}	Total Strain Tensor
δ_{ij}	Kronecker delta
ϵ_{ijk}	Levi-Civita symbol
α	Isotropic Coefficient Of Thermal Expansion
β	Isotropic Linear Variation Coefficient
$\lambda_0(\sigma)$	Stress Dependent Nonlinear Strain caused by the Magnetic Domain Rotation
λ_s	Saturated Magnetostriction
μ_o	Vacuum Permeability
k	Relaxation Factor
χ_m	Initial Susceptibility
η'	Isotropic Weiss Molecular Field Coefficient

χ	Auxiliary Vector Variable
K	Pinning Parameter
c	Reversible Coefficient
ξ	Variation of An hysteretic Magnetization as a Function of Effective Field
ρ	Mass Density
η_{el}	Elastic geometric factor
$\acute{\alpha}$	Ratio of crack length and width of SENB specimen
$\acute{\beta}$	Ratio of beam span and width of SENB specimen
φ	Magnetic scalar potential

Latin characters

s_{ij}	Stress Deviator Tensor
J_2	Second Invariant of Stress Deviator Tensor
I_σ	First Invariant of Stress Tensor
H_k	Magnetic Field Components
M_k or M_l	Magnetization Components
M_{an}	An hysteretic Magnetization
H_{eff}	Effective Magnetic Field
B	Magnetic Induction
E_{in}	Intrinsic Young's Modulus
ΔE	Variability in Young's Modulus
M_s	Saturation Magnetization
N_{kl}	Demagnetizing Factor
u_i	Displacements
f_i	Body Forces
P_{max}	Peak Fracture Load
J_{Ic}	Critical Strain Energy Release Rate
K_{Ic}	Fracture Toughness
\mathcal{W}	Strain Energy Density
\mathcal{T}	Kinetic Energy Density

X_1, X_2, X_3	Rectangular Cartesian Coordinates
S	Span of Specimen
W	Width of Specimen
a	Length of Single Edge Notch
B	Breadth of Specimen
P_f	Probability of Failure
P_u	Threshold Load Parameter
P_θ	Scale Parameter or Characteristic Strength Parameter
m	Distribution Shape Parameter or Weibull Modulus
R^2	Goodness of Fit
T	Ambient temperature
T_r	Easy axis transformation temperature
T_c	Curie temperature
N	Number of cycles

This Page is Intentionally Left Blank

Preface

The significance of the term “magneto-elastic fatigue and fracture” relevant to giant magnetostrictive materials in literature emphasizes the importance of such an analysis. Very few studies are performed related to evaluate the fracture and fatigue parameters, however all the concerning studies are limited to small number of experimental samples and piezomagnetic (linear) models. Evidently, the magneto-elastic response of the such giant magnetostrictive materials (e.g., Terfenol-D) is hysteretic, nonlinear and demonstrates the saturation phenomenon. The stress-strain relationship of Terfenol-D is bi-nonlinear in the absence of an applied magnetic field. This bi-nonlinear behaviour changes as the magnetization of the material increases, and the relationship becomes linear at saturation. Additionally, Terfenol-D shows the ΔE effect, which has nonlinear dependence on the stress and magnetic field. Thus, the nature of the failure in a bimodular material is influenced by the state of tension and compression regions in the flexure loading, which is largely neglected in existing literature. It is a well-recognized fact that the singular stresses are present near the crack front of a fracture process zone. In such cases, determining the position of the neutral axis is crucial to accessing the stress state singularity. When the stress-strain behaviour is different in tension and compression, it becomes tedious to determine a closed form solution accounting the singularity at the crack front. This happen to be a classical stress-dependent elasticity problem and additionally, for magnetostriction fatigue-fracture studies, the multi-physics of magnetic field domain must be coupled to the elasticity solution. It would be unwise to ignore this real field phenomena which might otherwise have caused many unwarranted failures in design of smart devices based on such materials. Also, the three-dimensional treatment is necessary to analyses this nonlinear fracture phenomenon. A robust fracture parameters prediction model for magneto-elastically coupled GMMs that will be appropriate for

numerical analysis, is required as the most potent driving force in GMMs fracture research.

The present work is primarily organised into two parts. The first part presents the theoretical framework including literature review and basic concepts of magneto-elasticity. In this part at first, a generalized nonlinear hysteretic thermo-magneto-elastic vector model of bulk giant magnetostrictive material is proposed using the thermodynamic relations coupled with the Taylor series expansion of Gibbs free energy density function for elastic deformation, the physics of demagnetization, and the Weiss molecular field. The magneto-thermo-elastic responses for rods/bars and, more importantly, for thin films/plates are numerically predicted and compared with the existing experimental ones in the literature for verification. The relative influence of magnetization, elastic, and thermal parameters on the coupled field response is characterized. Then, a 3-D path independent integral for mode I crack has been formulated. For maintaining the generality, the influence of magneto-thermo-elasticity is taken care of with the thermal strain, magnetic strain, and the magnetic body force terms. However, the present fatigue and fracture investigation is primarily focused on the magneto-elastic physics. This part serves as the foundation for next part.

The second part of this work details the experimental and numerical analysis plan to characterize the magneto-elastic response, and fatigue and fracture parameters of giant magnetostrictive material (i.e., Terfenol-D). At first, the magneto-elastic coupled field experimentation conducted for the procured Terfenol-D specimens to evaluate the magnetization, magnetostriction, and compressive stress-strain behaviour of the material as per the outlines mentioned in the respective ASTM standards. Then, the material properties are calibrated for the Terfenol-D specimens based on the physical and experimental evidence for magnetization and magnetostriction curves. The material

parameters are optimized to be further used in the constitutive model of the numerical fatigue and fracture analysis. Then an experimental study has been performed to characterize the fracture parameters of giant magnetostrictive material (GMM) in the coupled magneto-elastic field as per ASTM E399/E1820. The mean peak fracture load has been forecasted by using the two parameter Weibull statistical theory of strength. Then a numerical scheme is described to compute the fracture parameters of the Terfenol-D SENB specimen under an applied external field. A finite element model of the specimen has been created similar to the experimental one and the critical strain energy release rate J_{Ic} was calculated using the mean peak fracture load in both absence and presence of the external magnetic field. Finally, the three-point flexure fatigue experimental scheme that is used to evaluate the propagation of crack growth with the number of cycles in Terfenol-D SENB specimen with the absence and presence of an external magnetic field as per ASTM standards (i.e., E399 and E 647). A finite element simulation performed to determine the updated Paris law constants from the correlation of the crack growth rate with the values of ΔJ for a set of load ratio, magnetic field, and cyclic frequency. The experimentally and numerically evaluated fatigue failure data with the number of cycles spent were then compared to determine the validation and relevance of evaluated Paris law constants.

This Page is Intentionally Left Blank